



Li, Y., Gu, H., Pavier, M., & Coules, H. (2020). Compressive behaviours of octet-truss lattices. *Proceedings of the Institution of Mechanical Engineers, Part C: Journal of Mechanical Engineering Science*, 234(16), 3257-3269.
<https://doi.org/10.1177/0954406220913586>

Peer reviewed version

Link to published version (if available):
[10.1177/0954406220913586](https://doi.org/10.1177/0954406220913586)

[Link to publication record in Explore Bristol Research](#)
PDF-document

This is the author accepted manuscript (AAM). The final published version (version of record) is available online via SAGE Publications at <https://journals.sagepub.com/doi/abs/10.1177/0954406220913586?journalCode=picb>. Please refer to any applicable terms of use of the publisher.

University of Bristol - Explore Bristol Research

General rights

This document is made available in accordance with publisher policies. Please cite only the published version using the reference above. Full terms of use are available:
<http://www.bristol.ac.uk/red/research-policy/pure/user-guides/ebr-terms/>

Compressive behaviours of octet-truss lattices

Yifan Li, Huaiyuan Gu, Martyn Pavier, Harry Coules

Department of Mechanical Engineering, University of Bristol, Queen's Building, University Walk, Bristol BS8 1TR, UK

Abstract

Octet-truss lattice structures can be used for light-weighting in structural applications due to their high strength-to-density ratio. In this research, octet-truss lattice specimens were fabricated by stereolithography additive manufacturing with a photopolymer resin. The mechanical properties of this structure have been examined in three orthogonal orientations under compressive load. Detailed comparison and description were carried out on the deformation mechanisms and failure modes in different lattice orientations. Finite element models using both beam elements and 3D solid elements were used to simulate the compressive response of this structure. Both the load reaction and collapse modes obtained in simulations were compared with test results. Our results indicate that 3D continuum element models are required to accurately capture the behaviour of real trusses, taking into account the effects of finite-sized beams and joints.

Keywords

Octet-truss lattice, orientation-dependence, compression test, finite element simulation

1. Introduction

Lattice structures are used in industries such as aerospace, automotive and medicine because of their high strength-to-density ratios, high energy absorption and high porosity.¹⁻⁴ There are many ways to manufacture lattice structures, for example by casting, water-jet cutting, weaving and brazing.⁵⁻⁸ Recently, additive manufacturing techniques such as selective laser melting (SLM) and electron beam melting (EBM) have enabled direct fabrication of complex three-dimensional lattices from computer aided design (CAD) models.^{9, 10}

In general, the macroscopic mechanical properties of lattice structures are closely related to node connectivity.¹¹ Deshpande et al.¹¹⁻¹² concluded that stretch-dominated lattice structures generally have a higher specific efficiency compared to bending-dominated lattices and that for a structure to be stretch-dominated it should have a high nodal connectivity. The octet-truss lattice structure is a typical stretch-dominated lattice, with a unit cell of a nodal connectivity equal to 12.¹³ Octet-truss lattice structures have been already used in sectors including

aerospace, automotive, and medical applications. For example, they are used as an alternative to foams in lightweight structures, like sandwich panels, due to their higher strength-to-density ratio than bending lattices.¹² Mechanical properties of octet-truss lattices have been studied extensively using theoretical and experimental methods. Deshpande et al.¹² obtained closed-form expressions for the mechanical properties of FCC (Face-Centred Cubic) shape octet-truss lattices, such as modulus and strength. The octet-truss lattice is an anisotropic structure at the macroscopic level; the mechanical response is related to the structure's orientation. Their expressions were verified using experiments on aluminium alloy octet-truss lattices and FE simulation with good agreement.

O'Masta et al.¹⁴ investigated the relationship between fracture toughness and the relative density of octet-truss lattices using a lattice fabricated by a snap-fit and vacuum brazing method. They concluded that the fracture toughness of octet-truss lattices increases linearly with both the relative density and the square root of the cell size. Chen et al.¹⁵ proposed an analytical model that considers the effect of finite

sized joints between struts and the influence of bend and shear coupling to predict the compressive stiffness and strength of octet-truss lattices. Their analytical model was validated by finite element simulations and experimental results with varying relative densities. Chen et al.¹⁶ employed both experimental and numerical methods to research the mechanical behavior and energy absorption ability of octet-truss lattice under both quasi-static and dynamic compressive loading. The specific energy absorption (SEA) of octet-truss lattices manufactured from two different materials, brittle (standard grey resin) and ductile (durable resin), was compared with expanded polystyrene (EPS) foam. They showed that the brittle lattice structure has a low SEA, while the ductile lattice structure has a higher SEA but still lower than the EPS foam.

Recently, Gu et al.¹⁷ performed a numerical analysis to study the mechanical properties of octet-truss lattices in three different orientations. The study revealed the influence of lattice orientations on the mechanical behaviour, including modulus, strength and fracture toughness. Gu et al.¹⁸ also conducted fracture tests to investigate the orientation effects on octet-truss lattice fracture toughness and the crack paths, and the measured results were compared with the predicting results using Finite Element (FE) analysis. However, there are few studies on the effects of different orientations on the mechanical properties of octet-truss lattice structures, especially in experimental research. It is important to understand the mechanical response of octet-truss lattice structures with different orientations under compressive load, because the anisotropic lattice structures with different orientations often have different bearing capacities and mechanical reactions. Only with improved understanding of the mechanical response of octet-truss lattice structures with different orientations can they be better applied in lightweight supporting structures.

The present research aims to investigate the mechanical behaviour and compressive response of

octet-truss lattice in three different orientations (which will be defined in the next section) by using both experimental and finite element methods. Several lattice specimens manufactured by stereolithography (SLA) printing were investigated under compressive loading in three orientations. The deformation mechanisms and failure modes in three orientations were described in detail and compared with each other. The mechanical parameters such as elastic moduli, compressive strengths and Poisson's ratios were also obtained in the tests and compared with the FEM simulating results.

2. Experimental procedures

2.1 Specimen manufacture

Figure 1 presents the definition of lattice orientations and configuration of unit cell structure. The orientations were defined based on the loading direction and local coordinate of the unit cell. The theoretical relative density $\bar{\rho}_{th}$ of the lattice can be calculated using the first-order approximation:

$$\bar{\rho}_{th} = 6\sqrt{2}\pi(r/l)^2 \quad (1)$$

where r is the strut radius, and l is the strut length. The actual relative density $\bar{\rho}_{ac}$ can be obtained through experimental measurement by:

$$\bar{\rho}_{ac} = \frac{\rho_{lattice}}{\rho_{material}} \quad (2)$$

where $\rho_{lattice}$ is the density of the lattice structure and $\rho_{material}$ the density of the material of which the lattice is made. The tensile strength of the structure can be related to the relative density $\bar{\rho}$ and material failure strength σ_f by reference 17:

$$\sigma_t^I = C_I \bar{\rho} \sigma_f \quad (3)$$

where I equal to X, Y or Z, and C_I is a constant depending on the structure orientations and structure dimensions.

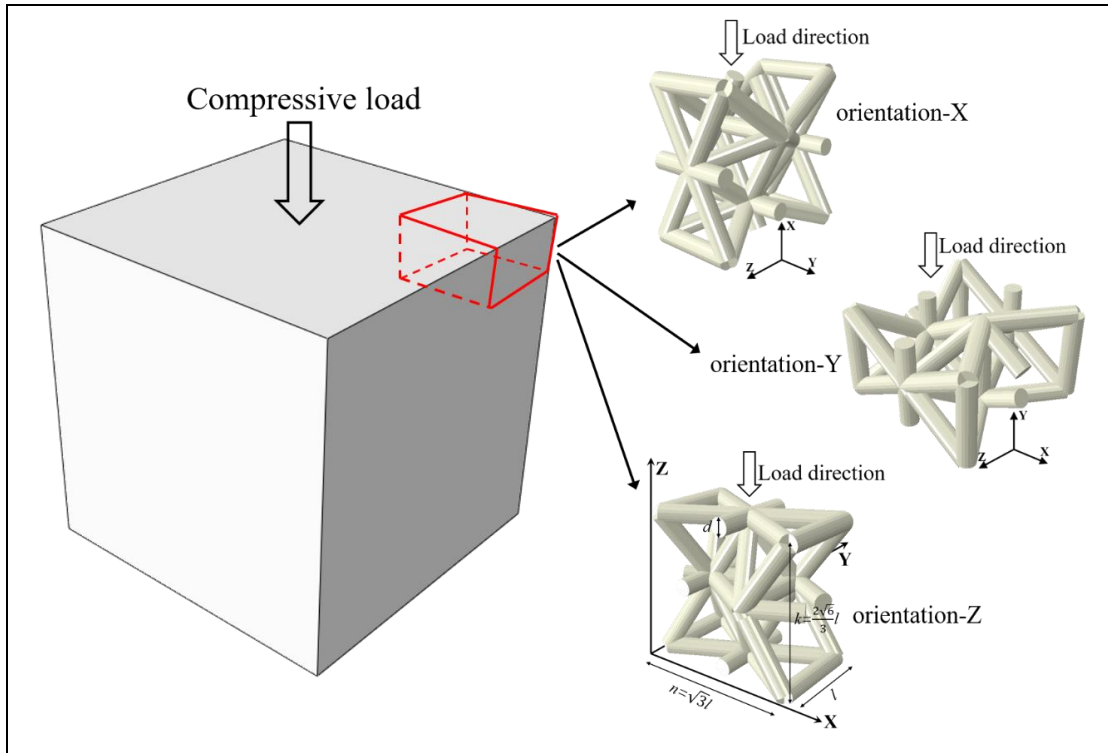


Figure 1. Definition of lattice orientations. The compressed solid represents the lattice structure and the cell orientations are defined by loading direction and local coordinate of the unit cell.

The geometry of the lattice specimen used in this work is shown in Figure 2. The designed nominal diameter of the struts is 2 mm and their nominal length is 10 mm. The overall designed dimensions of the specimen are 51.96 mm ×

48.99 mm × 50 mm to make sure at least three cells distributed in each side to reduce surface effects and the three sides of the specimen have similar size.

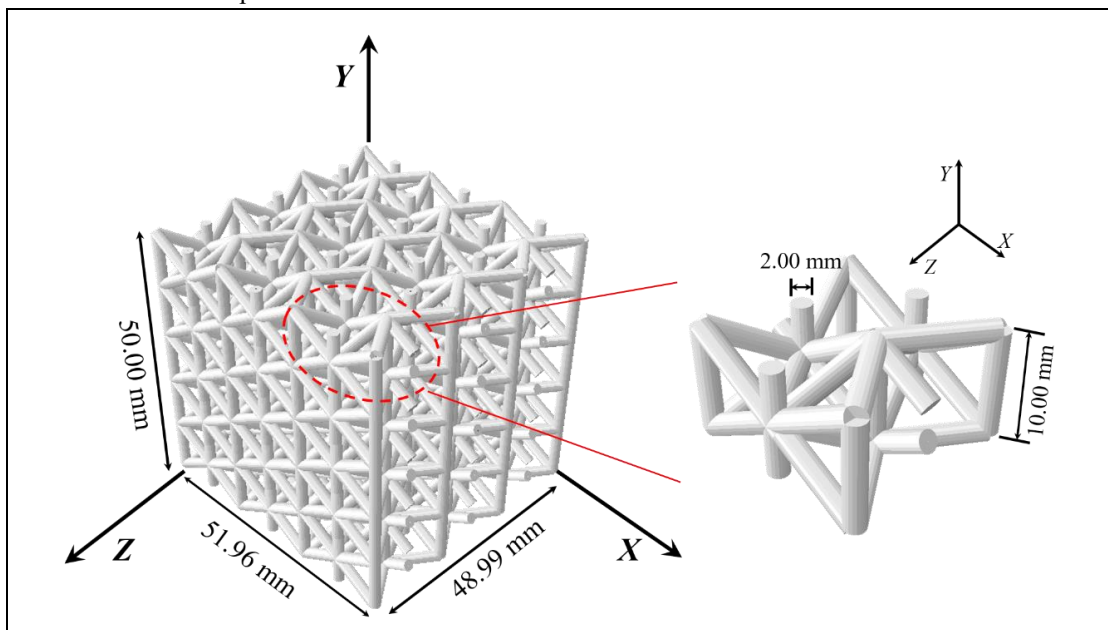


Figure 2. The designed dimensions of unit cell and lattice specimen. Left diagram shows the overall design dimensions of lattice structure and right diagram shows the design details for individual cell.

Stereolithography Apparatus (SLA) printing technique was used to manufacture this structure, because it has the advantage of high printing precise and smooth printing surface. SLA printing can be created high-quality samples cheaper than equivalent metal printing methods such as selective laser sintering (SLS) and selective laser melting (SLM). Individual struts in a SLA lattice structure exhibit excellent cross-sectional uniformity and mechanical uniformity.^{10,16} Therefore, SLA printing is a good choice for studying the mechanical behaviour of “perfect” lattice structures experimentally.

To manufacture the specimens, a three-dimensional lattice model was first designed using the Solidworks 2016.¹⁹ Next, the STL file produced by the CAD software was imported into a ZRapid iSLA 660 3D printer machine to be sliced into 2D layers. Finally, the ZR680 photopolymer resin was converted from liquid into 3D solid plastics in a layer-by-layer fashion by using high-powered ultra-violet (UV) laser. The 3D

printer had layer resolution ranging from 50 to 100 μm , controlled by the optical size of the UV laser. In this study, a 50 μm layer resolution was used to print all the specimens. The laser power was set to 3000 mW. After printing, the specimens were cleaned in a solution (95% ethanol) to remove support material and flash. After being washed, the specimens were placed in a UV oven for further hardening. The SLA printing machine used in this research and the schematic diagram of stereolithography setups are shown in Figure 3. All printed specimens had a smooth surface after post-processing. The mean dimensions of the nine specimens, measured using digital calipers, are 49.85mm \times 47.75mm \times 47.77mm (contrast with the designed dimensions in Figure 2). The mean diameter of the individual strut measured by total 27 struts in different sides of nine specimens is 2.1mm. The theoretical relative density calculated using equation (1) and measured actual relative density are presented in Table 1.

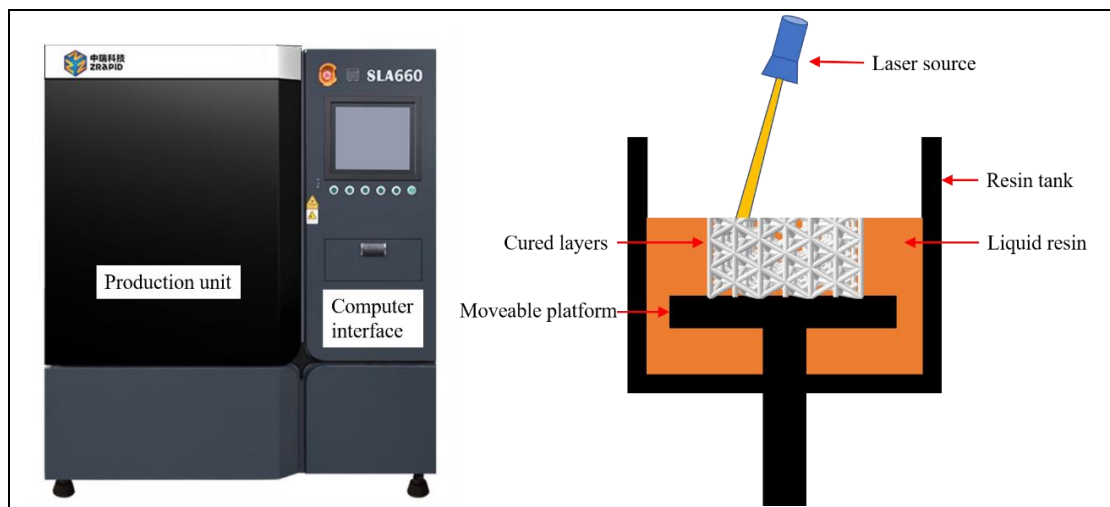


Figure 3. The ZRapid iSLA 660 printer (left) and a schematic diagram of stereolithography setup (right). At the beginning of printing, the platform is a little below the liquid resin, where the UV laser then hardens the first layer. Next, the platform moves a little further below resin, and layering process repeats until a complete 3D object is formed.

Table 1. Relative density of octet-truss lattice

designed strut dimension, r/l	mean volume, cm^3	mean mass, g	$\bar{\rho}_{th}$	$\bar{\rho}_{ac}$
1/10	113.71	36.96	0.267	0.262

2.2 Mechanical testing of basic material

Material properties of the 3D printed

photopolymer resin were determined by tension and compression tests on solid specimens. Tensile

specimens according to ASTM D638 and cylindrical compressive specimens with ASTM D695 were 3D printed using the same printing parameters as the

lattice specimens.²⁰⁻²¹ The dimensions of these specimens are shown in Figure 4.

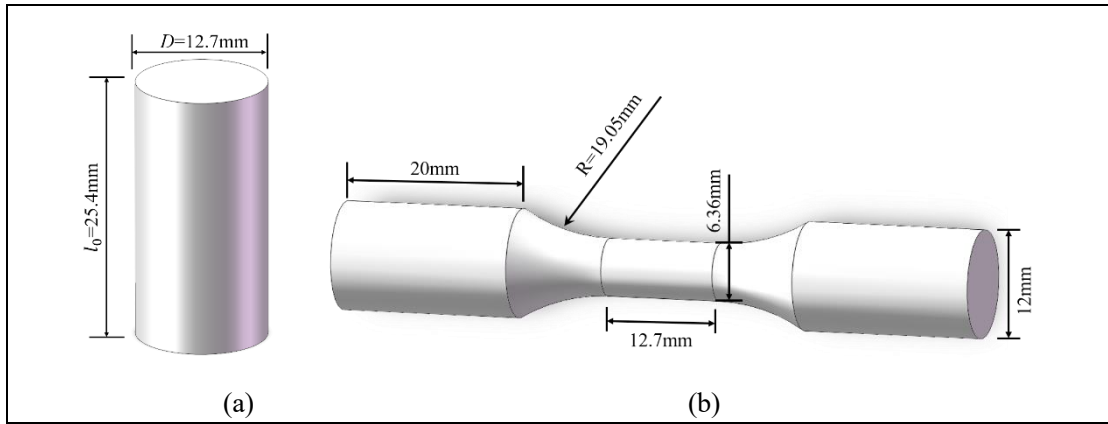


Figure 4. The dimensions of compressive specimen (a) and tensile specimen (b).

Tensile tests were performed using an Instron 8872 hydraulic test machine equipped with a 25 kN load cell. Displacement control was used with a rate of 1.25 mm/min. Three specimens were tested using the same test conditions. A Zwick Roell 1466 test machine equipped with a 50 kN load cell was used for the compressive tests. Displacement control was used with a rate of 1.3 mm/min. Five cylindrical specimens were tested with a mean diameter $D=12.7$ mm and initial length $l_0=25.4$ mm. Several different factors affect mechanical properties in stereolithography printing, and size effect and thickness effect have the insignificant influences.²²⁻²⁴ The individual lattice struts are small, which would make it challenging to perform accurate tensile tests. Therefore, the printed standard test specimens were used as a substitute to obtain a mechanical response representative of strut

elements.

Figure 5 presents the engineering stress-strain curves for the 3D printed material. In the tensile tests a toe region was observed in the test results. This region was removed for the results presented in Figure 5 using the procedure described in ASTM D638.²⁰ During the material tests, the specimen failed at a relatively small strain under tensile load, while under compressive load the cylindrical specimen only showed the typical barreled shape and no shear failure occurred. Only part of the compression curve was shown in Figure 5, because the complete compressive curve has large compressive strain and if the scope of x-axis is too large to visually show the performance of tensile curve. The material properties measured in the tests are compared with those obtained from the material supplier in Table 2.

Table 2. Mechanical properties of basic material

	Modulus E , GPa	Tensile strength, MPa	Failure strain	Poisson's ratio	Density g/cm^3
Measured	2.415	58	0.05	—	1.24
Supplier	2.500~3.000	45~54	0.11~0.2	0.23	1.3

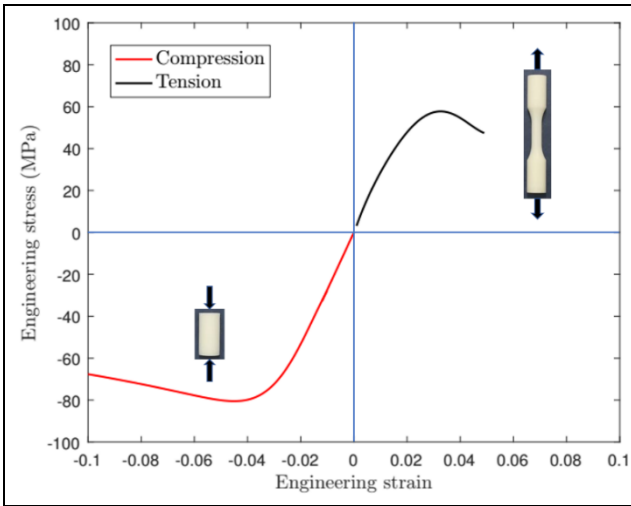


Figure 5. Stress-strain curves of 3D printed material. The curve in upper right of the graph represents the tensile response of material, while the bottom left curve is only part of the compression curve and cylindrical specimens

did not break during the compression test.

2.3 Compression tests of lattice structure

Compression tests of lattice specimens for the three different orientations were carried out using a Zwick Roell 1466 testing machine using displacement rate of 1.3mm/min. Three specimens were tested for each orientation. An iMETRUM video gauge system was used to record the displacements of a sequence of reference points, as shown in Figure 6 for a Y-orientation compressive specimen.²⁵ These displacements were used to calculate the Young's moduli and Poisson's ratios of the structures. Individual frames from the videos were also extracted to illustrate the mechanisms of progressive collapse of the structures as shown in Section 4.

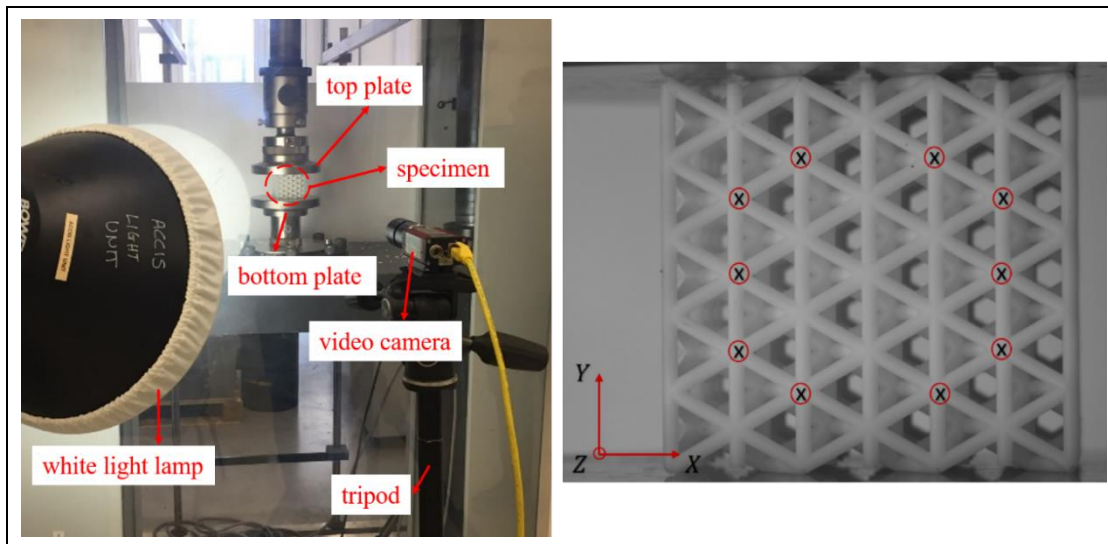


Figure 6. Lattice compressive tests (left) and example of reference points (right). The data from middle two columns was used to calculate longitudinal strain of lattice structure and data from three rows was used for transverse strain. The ratio of strains in the elastic regime gives the Poisson's ratio.

3. Finite element simulation

Finite element models of three-dimensional lattice structures usually either use beam elements or 3D solid elements. A model using beam elements has much lower computational cost but it is difficult to accurately model manufacturing defects and the detailed geometry of joints between the struts.²⁶ Attempts have been made to address the problems caused by the use of beam elements. Each strut may be discretized using several beam elements with different

properties to model more accurately 3D printed struts with varying cross-sections.²⁷⁻²⁸ Labeas et al.²⁹ increased the diameter for each strut near its ends to model better geometry of the joints, while Luxner et al.³⁰ achieved the same result by increasing the material modulus in the vicinity of the joints.

The commercial FEA software Abaqus 2017 version was used to simulate the response of the octet-truss lattice to compressive load in order to evaluate numerical deformation behavior with the experimental

data.³¹ The explicit dynamics procedure was used in numerical analysis and geometrical nonlinearity was taken into account. The photopolymer resin used to fabricate lattices was modelled as an elastic plastic material with isotropic hardening. The material data was obtained from the uniaxial tests in Table 2, where the density is 1.24 g/cm^3 , Young's modulus is 2.415 GPa , Poisson's ratio is 0.23 and the yield strength is 54.06 MPa . Element deletion method was used to model the strut failure in tests. Failure initiates when the maximum strain in the element reaches 0.032 which is obtained from the tensile test. The degradation of the material stiffness was described by a damage variable B , when $B = 1$ the material point has completely failed and the corresponding element is deleted from the model. Beam elements and solid elements were both used to model the lattice structure. Two beam element models were used. In the first beam element model the diameter of the struts was set to 2.1 mm to match the measured diameter of the struts. In the second model, the diameter of the struts was increased to 2.94 mm over for the last 1 mm of the

length of each strut, following the method of Labeas et al.²⁹ In these two beam models, each strut is meshed by using three dimensional, shear deformable, linear beam element B31 with 1 mm seed size to consider the transverse shear deformation of short strut. For the solid element model, a 4-node linear tetrahedral element C3D4 was used with 0.5 mm seed size. In these simulations, 2D beam element models contained approximately 12000 elements and 3D solid element models had nearly 2600000 elements.

Two rigid plates were created to apply a vertical displacement as the experiment to the lattice model. A fixed displacement condition over all degrees of freedom was applied in the lower free surface of lower rigid plate, and the upper plate can move along the load direction. A hard contact condition was used between the plates and the lattice structure. The contact property in tangential direction between plates and lattice was identified as frictionless, because of the smooth surfaces of lattice struts and metal plates. Figure 7 shows the FE models of a unit cell from the specimen for different elements.

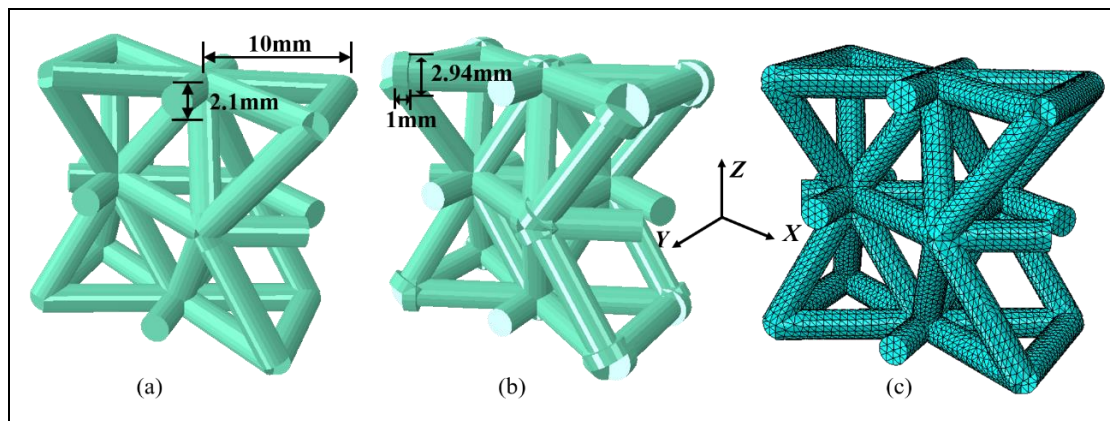


Figure 7. FE models for different elements: (a) beam element, (b) beam element with material concentration, and (c) solid element. An individual strut in both beam models consists of ten beam elements, and the solid element model has a mesh seed size of 0.5 mm .

4. Results and discussion

4.1 Experimental results and failure mechanisms

Since the 3D printed photopolymer resin used in the tests exhibited distinctly brittle performance, the lattice specimens ruptured as soon as the struts reached the critical strain, so no densification phenomenon

happened during the tests. In order to study the structure's mechanical response, the nominal stress and nominal strain of lattice structure were defined to distinguish from localized stress and strain in lattice individual struts. Nominal stress and strain are the applied parameters of lattice structures, which should be calculated by dividing the lattice structure's

dimensions (engineering strain stress for the whole specimen). Figure 8 depicts the nominal stress-strain curves of representative octet-truss lattice specimens in three different orientations under compression load. In octet-truss lattice structures, applied load is generally carried by struts under tension and compression, while the bending struts have a second order effect on lattice strength.¹⁷ The stress states of unit cell under compressive load according to the analytical model in reference 17 is illustrated in Figure 9, in which red, blue and grey colours respectively represent struts under tension, compression and bending-dominated conditions. The analytical model is an individual cell derived from the infinite lattice structure. Although the stress distribution in this model will vary from that of any individual cell in an actual lattice structure, it will roughly reflect the mechanical behaviour of the structure in the elastic regime. For example, Gu et al.¹⁷ have used a single-cell model of this type to obtain the theoretical strength of infinite octet-truss lattice structures in different orientations. As shown in Figure 9, most of the struts in Z-orientation mainly under tension and compression, while only a few vertical struts in Y-orientation under compression dominated. Therefore, Z-orientation has the maximum load bearing capacity and Y-orientation has the minimum one, which can be validated by test results in Figure 8. The compressive strength and

standard deviations of all lattice specimens is shown in Table 3; the compressive strength values have low scatter. The mean compressive strengths of lattice structure measured in X, Y and Z orientations are 4.25 MPa, 3.50 MPa and 5.32 MPa, respectively. The tensile strength of the material is 58 MPa (see Table 2). Equation (3) was used to normalize the compressive strength and obtain the dimensionless parameter C_L , which defined as normalized strength, for different orientations are 0.28, 0.23 and 0.35.

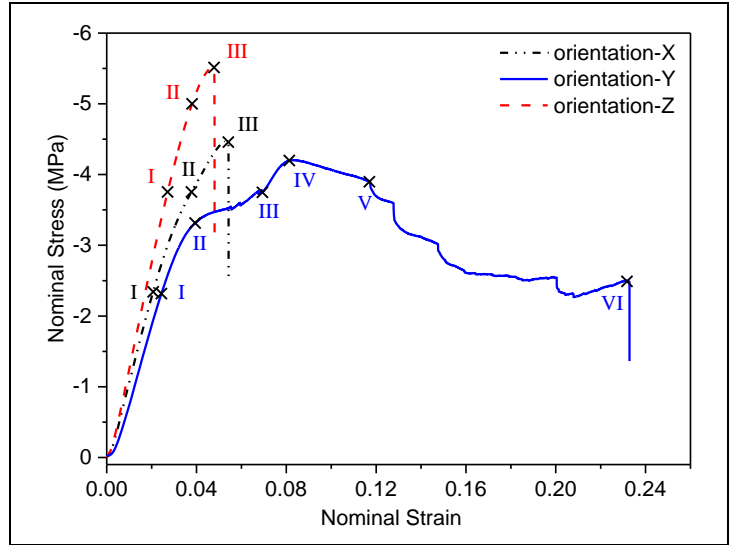


Figure 8. Compressive stress-strain curves of octet-truss lattice in different orientations. The roman numerals correspond to the deformation conditions shown in Figure 10.

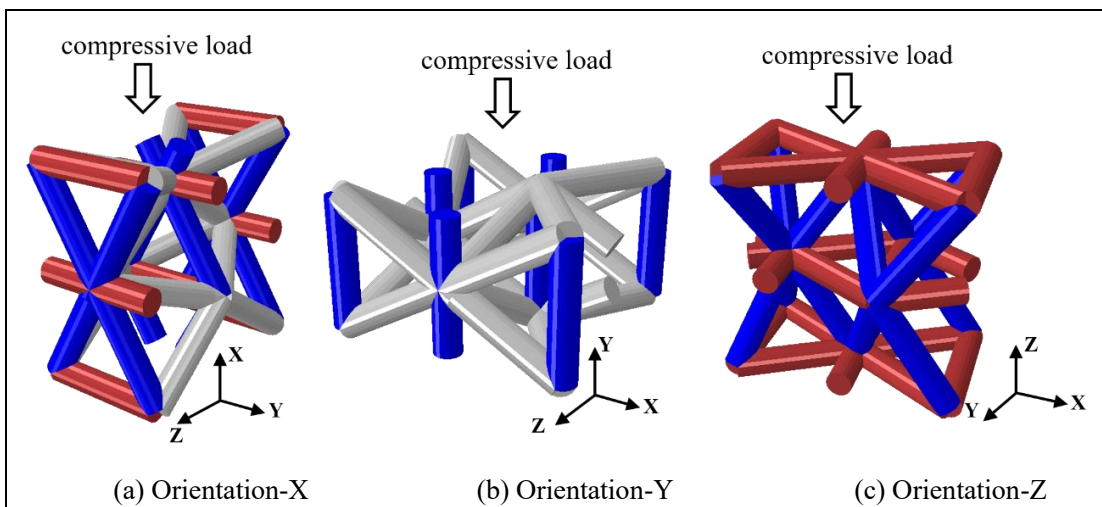


Figure 9. Octet truss unit cell under compression. Red indicates struts mainly under tension, blue indicates struts mainly under compression, and grey indicates struts mainly under bending.

Table 3. Compressive strengths of lattices in different orientations. (SD means Standard Deviation)

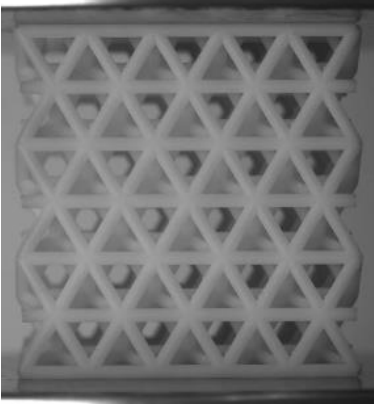
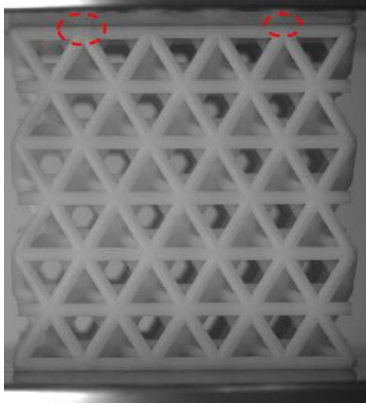
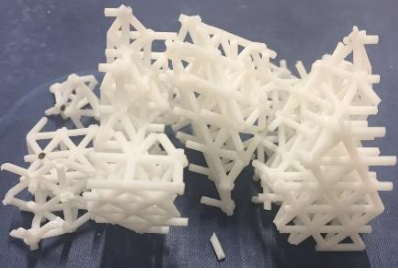
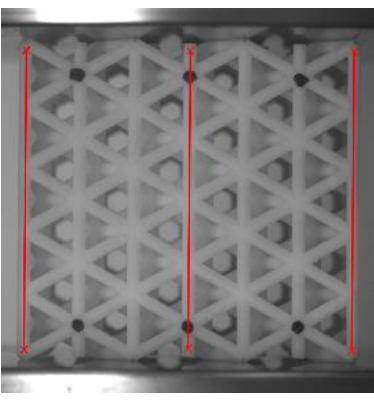
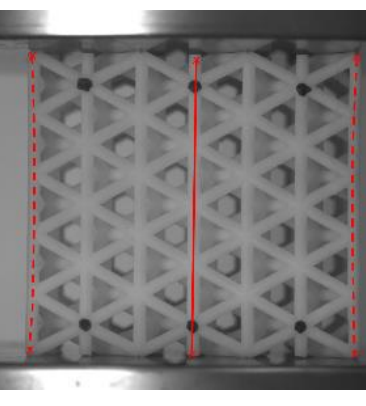
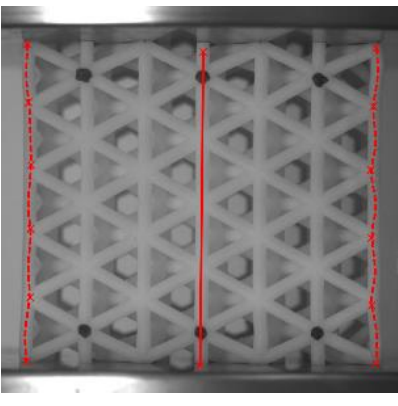
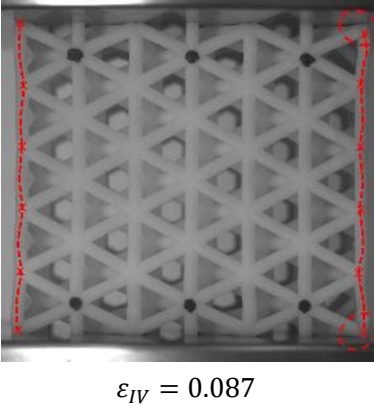
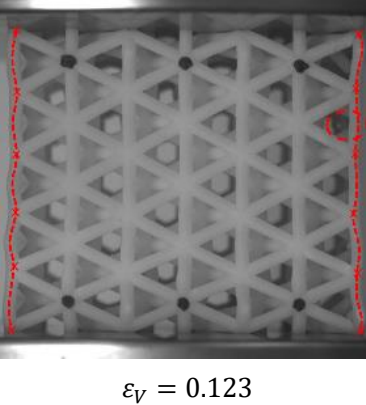
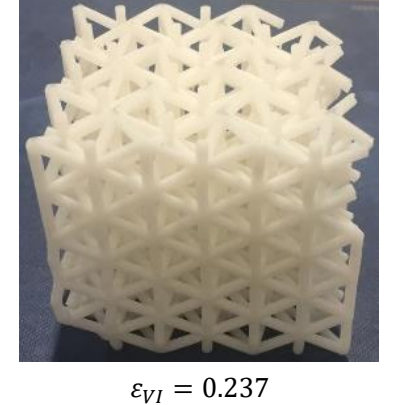
Orientation	Specimen number	Compressive strength (MPa)	Mean compressive strength and SD
X	1	4.25	4.25 (0.086)
	2	4.36	
	3	4.15	
Y	1	3.64	3.50 (0.191)
	2	3.63	
	3	3.23	
Z	1	5.54	5.32 (0.337)
	2	5.57	
	3	4.84	

In order to better understand the deformation process of specimens with different orientations, individual frames extracted from videos are presented in Figure 10. Figure 10 illustrates the deformations of lattices and the associated nominal strain, as well as the failure modes and failure strain. The subscripts of the strain in these figures correspond to the main stages in Figure 8. Lattice structures in X and Z orientations both went through three steps of failure. In the compression process of X and Z orientations, the structures initially experienced a linear elastic phase and then a nonlinear one. Finally, the lattice structures failed explosively. Octet-truss lattice made by photopolymer resin exhibited typical brittle behavior in X and Z orientations. During the compression procedure, X and Z orientations show similar deformation patterns in different layers. After the linear elastic phase in orientation-X, damage initiated at the strut joints where stress concentrations

happened, shown in red circles in Figure 10(b). Finally, the lattice structure in orientation-Z broke drastically into more pieces than orientation-X, because more struts in orientation-Z under tension than that in orientation-X and known from Figure 5 that the failure mode of photopolymer resin used in the tests is tensile failure.

The failure of lattice structures in orientation-Y has a more complex mechanism. Dashed red lines are drawn to the center of the struts at the boundary of specimen to emphasize the deformation pattern of these struts. After a linear elastic phase, the vertical struts in the left and right sides acted as one column, which became unstable and buckling occurred, as shown in Figure 10(e). As the experiment went on, deformation of vertical struts at the edge of structure was constrained by inclined struts, so the edge vertical struts began to buckle individually and the load capacity increased slightly presented in Figure 10(f). Because different column with the same cross-section, if the column is shorter the Euler's critical load is larger. After this, when the compressive load reaching the peak value, damage initiated at the struts where the specimen contacted with compression plates shown in Figure 10(g) in red circles. In Figure 10(h), a red circle denotes that some struts failed and separated from the lattice structure, then the reaction force decreased instantly corresponding to step V in Figure 8. The failure mode of orientation-Y lattice is stable buckling failure of edge struts with part of struts crushed in the lattice structure, so the specimen can still be intact. In general, the failure of the broken struts starts at the top or bottom layers where specimen is contact with the compression plates in Y orientation.

Orientat ion	Deformation procedure
-----------------	-----------------------

X	 <p>$\varepsilon_I = 0.023$ (a)</p>	 <p>$\varepsilon_{II} = 0.040$ (b)</p>	 <p>$\varepsilon_{III} = 0.056$ (c)</p>
Y	 <p>$\varepsilon_I = 0.030$ (d)</p>	 <p>$\varepsilon_{II} = 0.045$ (e)</p>	 <p>$\varepsilon_{III} = 0.075$ (f)</p>
	 <p>$\varepsilon_{IV} = 0.087$ (g)</p>	 <p>$\varepsilon_V = 0.123$ (h)</p>	 <p>$\varepsilon_{VI} = 0.237$ (i)</p>

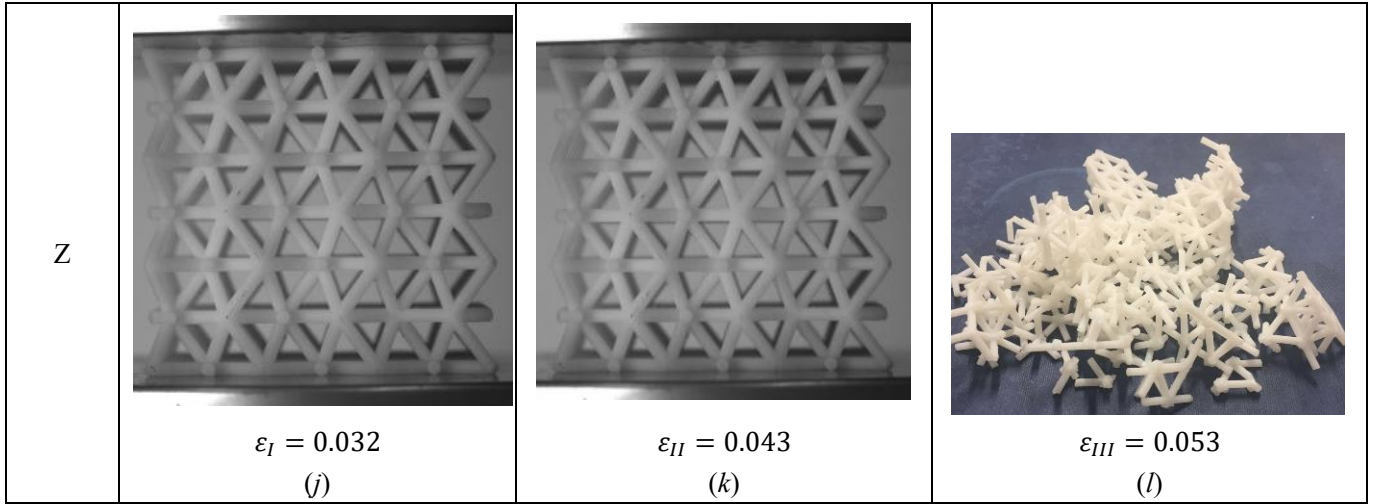


Figure 10. Deformation modes of octet-truss lattice specimens: (a)–(c) Orientation X, (d)–(i) Orientation Y, (j)–(l) Orientation Z. Orientations X and Z exhibit semi-brittle failure and red circles represent locations where failure first initiates in strut joints. Orientation Y exhibits ductile behaviour. Red dashed lines show the deformation pattern of selected struts.

The stress-strain responses of these lattices are complicated. In order to obtain the elastic modulus of lattice on different orientations, the relationship between stress gradient and strain of different orientation lattices was acquired using secant method for the adjacent data points. The stress gradient changing with strain is shown in Figure 11. The linear elastic region of the lattice specimens following the increasing gradient below 0.01 strain, which is due to the full contact between specimen and compressive platen. All the three orientations lattice have linear elastic reaction between 0.015 and 0.025 strain, so the elastic moduli are extracted from this region. The mean elastic moduli of X, Y and Z orientations lattice are 127.99MPa, 114.48MPa and 145.52MPa, respectively. Like the normalized compressive strengths, the normalized elastic moduli can also be calculated by a similar formula $E_{exp}/(\bar{\rho}E_S)$. The elastic modulus of this material measured is 2.415 GPa, so normalized moduli for X, Y and Z orientations are 0.20, 0.18 and 0.23.

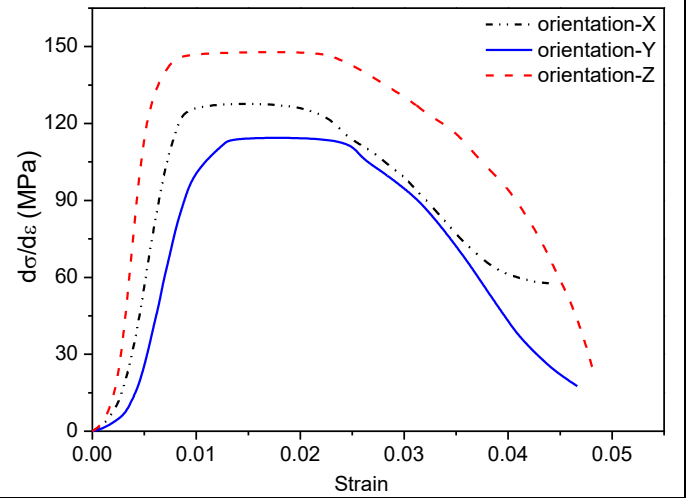


Figure 11. The stress gradient of lattices on different orientations. The increasing gradient below 0.01 strain due to the full contact between specimen and compressive platen.

The Poisson's ratios of different orientations were also calculated by using the transverse strain divided the vertical strain obtained from video gauge data. The same surface was photographed by the video gauge in orientations X and Y, so only two Poisson's ratios, i.e. v_{xy} and v_{xz} , were obtained in this study. According to the definition of Poisson's ratio, it is only for linear elastic deformations. The Poisson's ratios measured in the tests became stabilized and gradually asymptotic to a stable value when the strain of

specimens near 0.015, and the specimens have strain between 0.015 to 0.025 are linear elasticity. Therefore, the measured ν_{xy} and ν_{xz} between this linear elastic strain range are 0.37 and 0.24 the Poisson's ratios of lattice specimens.

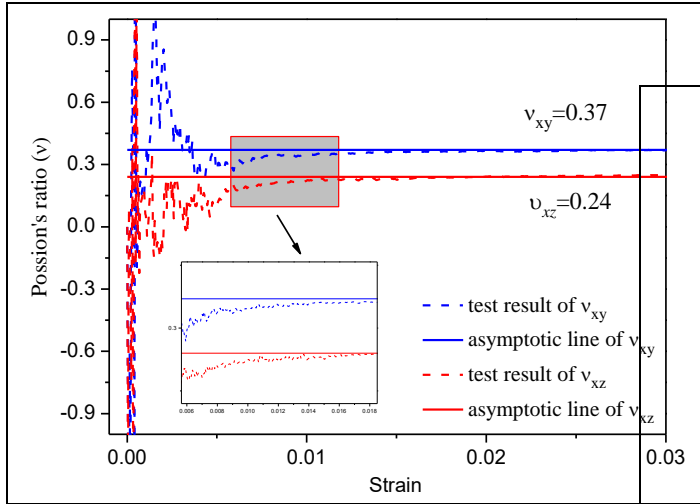
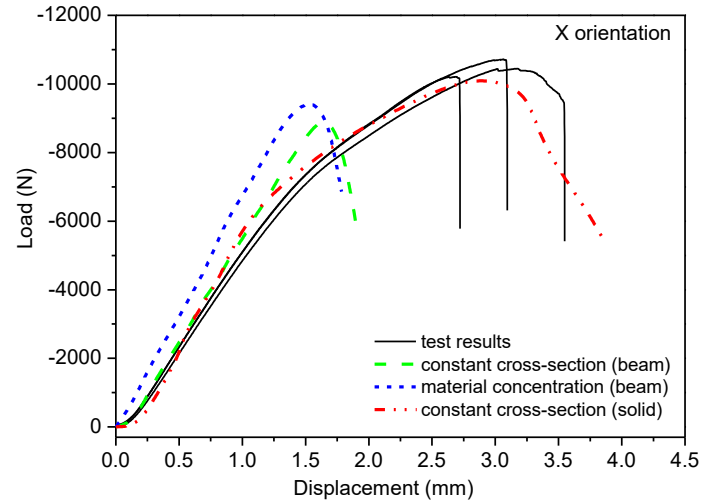


Figure 12. Poisson's ratios for different orientations. The dashed lines (blue and red) represent the change of Poisson's ratio measured by the experiment. The fluctuation of the measured Poisson's ratios is due to full contact being made between the specimens and compressive platen.

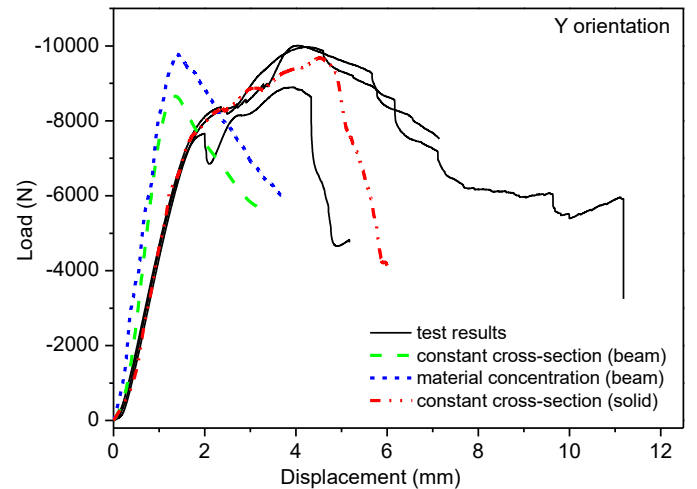
4.2 Simulation results and evaluation

In this section, the simulation results of different element types and comparisons are presented. Figure 13 illustrates the mechanical response of lattice structure in different orientations, and negative value represents compressive load. The displacement and reaction force data were obtained from the reference point of the upper rigid plate. It can be observed from Figure 13 that the finite element results of solid element are in good agreement with the experimental results in all three orientations. The solid model predicts the initial stress, elastic stiffness and compressive strength values are in accordance with the experimental results. In the contrast, beam element can only predict well the elastic region, and the predicted collapse strain smaller than the test results. For constant cross-section beam model, the predicted critical loads of lattice failure are also smaller than the real values, and the material concentration beam models can obtain more accurate results. Beam models with a finer mesh were also performed to exclude the

effect of mesh size on results. This demonstrated that the use of a finer mesh did not significantly affect simulation. The comparison between predicted mechanical parameters from solid element and experimental results are shown in Table 4, and the numerical predictions agree well with the experimental results.



(a)



(b)

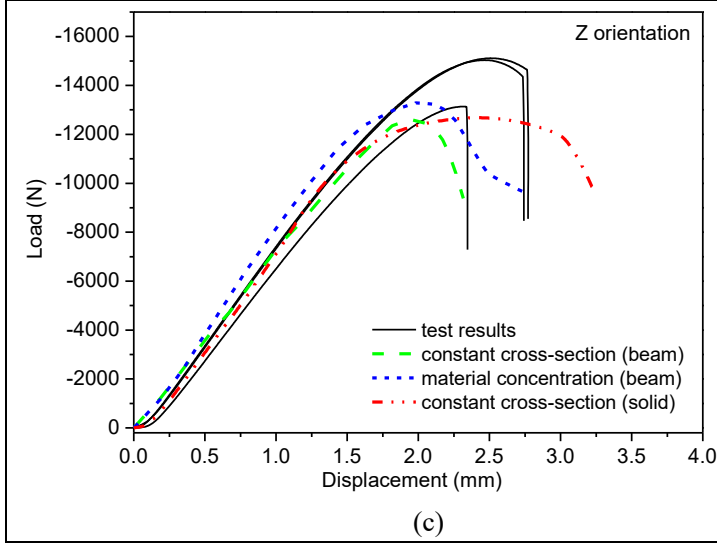


Figure 13. Load-displacement curves for different lattice orientations: (a) Orientation-X, (b) Orientation-Y, (c) Orientation-Z. The green and blue lines (represent beam models) reach the extreme values and drop earlier than the red line (solid model) because some struts in the models collapsed in advance during compression.

Table 4. The comparison of measured mechanical parameters with solid element model predictions

Mechanical property	Orientation-X	Orientation-Y	Orientation-Z
$E_{exp}/(\bar{\rho}E_s)$	0.20	0.18	0.23
$E_{FE}/(\bar{\rho}E_s)$	0.22	0.22	0.20
$\sigma_{exp}/(\bar{\rho}\sigma_f)$	0.28	0.23	0.35
$\sigma_{FE}/(\bar{\rho}\sigma_f)$	0.30	0.22	0.33
Poisson's ratio	ν_{xy}	ν_{yz}	ν_{xz}
ν_{exp}	0.37	—	0.24
ν_{FE}	0.33	0.15	0.25

* σ_{exp} is the measured lattice compressive strength and σ_{FE} is the FE predicted compressive strength

The deformation patterns of experimental results compared with finite element results under the related

strains are presented in Figure 14. The lattice deformation was adequately predicted by the model using solid elements, including the uniform deformation in X and Z orientations and buckling of edge struts in the Y orientation. In contrast, the simulating results using beam elements in orientation-X crushed in the top layer, and the deformation model in orientation-Y was observed that a shear band at 60° was formed during the compressive process. The deformation prediction of beam element in Z orientation was well agreed with the experimental result if the collapse of some struts in the central layer was disregarded. This response was also reflected in

the load–displacement curves in Figure 13, and beam model in orientation-Z can predict a better load trace comparing with orientation-X and orientation-Y beam models. The first reason that the beam models do not reflect the mechanical response of this lattice structure is that the geometry of joints cannot be accurately modeled. Also, beam elements do not satisfy the struts have large strut slenderness ratio (d/L). According to the beam theory used in Abaqus, shear flexible beam theory can provide useful results for slenderness ratio up to 1/8. Beyond this ratio, the approximations that allow the member's behavior to be described solely as a function of axial position no longer provide adequate accuracy.³² Ahmadi et al. have researched the apparent density effects on the mechanical properties of diamond-type lattice structures, showing that with the increase of apparent density, i.e. the slenderness ratio of lattice struts gets larger, the beam element simulation results deviated from the experimental results.³³ Dong et al. also showed that beam elements are not applicable to stout struts because the assumption of beam element requires slender struts.²⁶ Therefore, 3D solid elements are recommended to model the lattices have struts with large slenderness ratio.

Orientation n	Experiment	Beam element model	Solid element model
---------------	------------	--------------------	---------------------

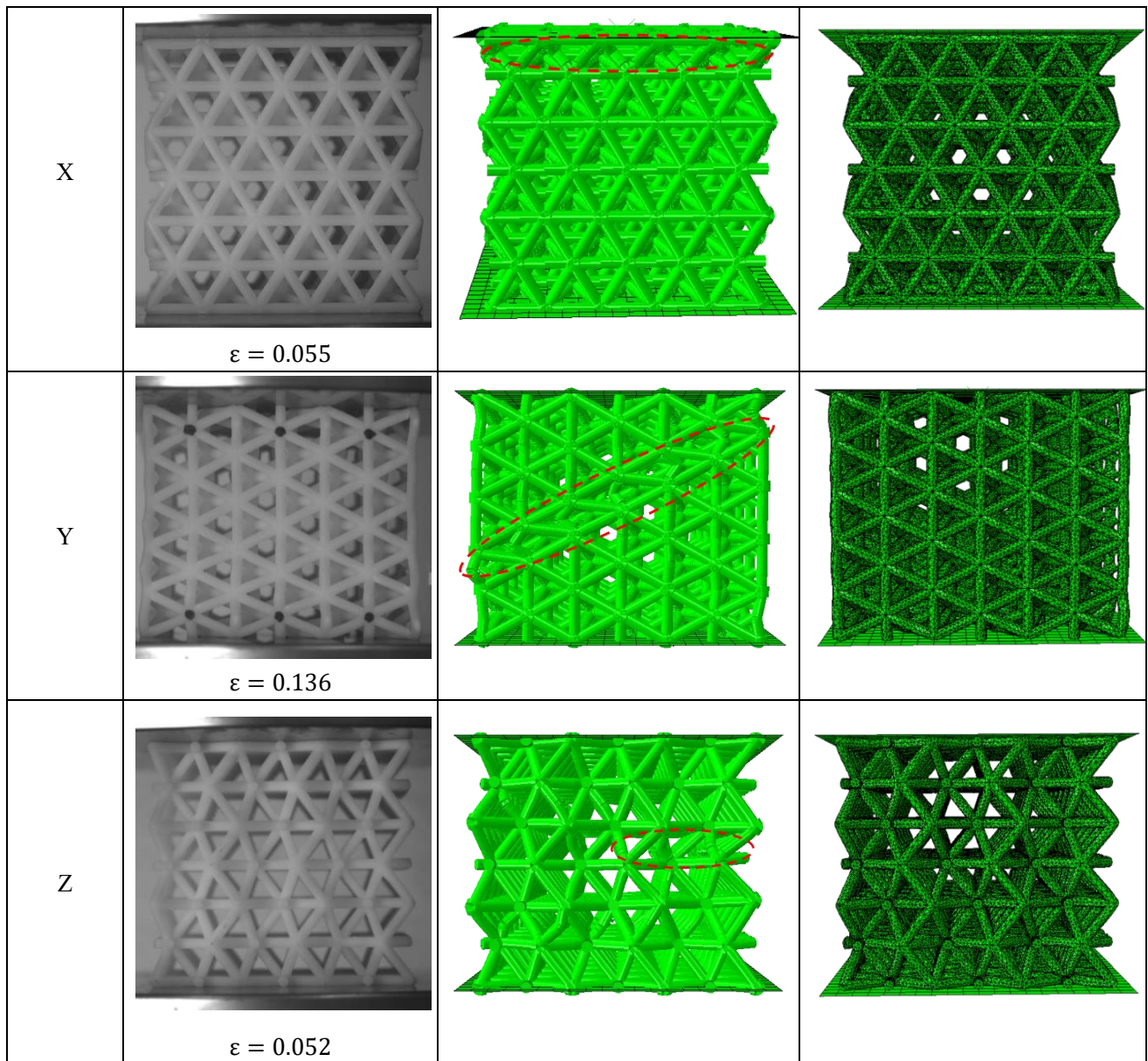


Figure 14. The comparison of deformation patterns between experiments and simulations. Images in the middle column shown simulation results from beam model with material concentration, which have similar deformation patterns with normal beam model. The right column shows results from solid element model (at the the same strain).

5. Conclusion

The orientation effects on mechanical properties of octet-truss lattice structure, made of photopolymer resin by Stereolithography Apparatus (SLA), were studied using experimental testing and finite element simulation. Octet-truss lattice structures in orientation-Z and orientation-X have better load bearing capability and fail at small nominal strain, while this structure in orientation-Y has the opposite performance. The normalized compressive strengths of this structure

made of photopolymer resin in X, Y and Z orientations measured are 0.28, 0.23 and 0.35, respectively. Simulation results from solid element models have better agreement with the experimental results than those from 3D beam element models, both in terms of the mechanical responses and deformation patterns in all three orientations. Mechanical parameters such as Poisson's ratios, normalized elastic moduli and compressive strengths obtained from the solid element models agree very well with the results measured from

tests in all three orientations.

Declaration of Conflicting Interests

The author(s) declared no potential conflicts of interest with respect to the research, authorship, and/or publication of this article.

References

1. Banhart J. Manufacture, characterisation and application of cellular metals and metal foams. *Prog Mater Sci* 2001; 46(6): 559-632.
2. Hedayati R, Janbaz S, Sadighi M, et al. How does tissue regeneration influence the mechanical behavior of additively manufactured porous biomaterials? *J Mech Behav Biomed Mater* 2017; 65: 831-841.
3. Bobbert FSL, Lietaert K, Eftekhari AA, et al. Additively manufactured metallic porous biomaterials based on minimal surfaces: A unique combination of topological, mechanical, and mass transport properties. *Acta Biomater* 2017; 53: 572-584.
4. Zheng X, Lee H, Weisgraber TH, et al. Ultralight, ultrastiff mechanical metamaterials. *Science* 2014; 344(6190): 1373-1377.
5. Li Q, Chen EY, Bice DR, et al. Mechanical properties of cast Ti-6Al-4V lattice block structures. *Metall Mater Trans A* 2008; 39(2): 441-449.
6. Dong L, Deshpande V, Wadley H. Mechanical response of Ti-6Al-4V octet-truss lattice structures. *Int J Solids Struct* 2015; 60: 107-124.
7. Wadley HNG, Fleck NA, Evans AG. Fabrication and structural performance of periodic cellular metal sandwich structures. *Compos Sci Technol* 2003; 63(16): 2331-2343.
8. Helou M, Kara S. Design, analysis and manufacturing of lattice structures: an overview. *Int J Computer Integr Manuf* 2018; 31(3): 243-261.
9. Wauthle R, Vrancken B, Beynaerts B, et al. Effects of build orientation and heat treatment on the microstructure and mechanical properties of selective laser melted Ti6Al4V lattice structures. *Addit Manuf* 2015; 5: 77-84.
10. Huynh L, Rotella J, Sangid MD. Fatigue behavior of IN718 microtrusses produced via additive manufacturing. *Mater Des* 2016; 105: 278-289.
11. Deshpande VS, Ashby MF, Fleck NA. Foam topology: bending versus stretching dominated architectures. *Acta Mater* 2001; 49(6): 1035-1040.
12. Deshpande VS, Fleck NA, Ashby MF. Effective properties of the octet-truss lattice material. *J Mech Phys Solids* 2001; 49(8): 1747-1769.
13. Fuller RB. Octet Truss. Patent Serial No. 2 986 241, USA, 1961.
14. O'Masta MR, Dong L, St-Pierre L, et al. The fracture toughness of octet-truss lattices. *J Mech Phys Solids* 2017; 98: 271-289.
15. Chen XY, Tan HF. An effective length model for octet lattice. *Int J Mech Sci* 2018; 140:279-287.
16. Ling C, Cernicchi A, Gilchrist MD, et al. Mechanical behaviour of additively-manufactured polymeric octet-truss lattice structures under quasi-static and dynamic compressive loading. *Mater Des* 2019; 162: 106-118.
17. Gu H, Shterenlikht A, Pavier M. Brittle fracture of three-dimensional lattice structure. *Eng Fract Mech* 2019; 219: 106598.
18. Gu H, Li S, Pavier M, et al. Fracture of three-dimensional lattices manufactured by selective laser melting. *Int J Solids Struct* 2019; 180: 147-159.
19. DSS Solidworks. Das-sault Systems SolidWorks Corp, Concord, MA, USA, 2016.
20. ASTM D638-14:2015. Standard Test Method for Tensile Properties of Plastics.
21. ASTM D695-15:2015. Standard Test Method for Compressive Properties of Rigid Plastics.
22. Chockalingam K, Jawahar N, Chandrasekhar U. Influence of layer thickness on mechanical properties in stereolithography. *Rapid Prototyp J* 2006; 12(2): 106-113.
23. Yang Y, Li L, Zhao J. Mechanical property modeling of photosensitive liquid resin in stereolithography additive manufacturing: Bridging degree of cure with tensile strength and hardness. *Mater Des* 2019; 162: 418-428.
24. Puebla K, Arcaute K, Quintana R, et al. Effects of environmental conditions, aging, and build orientations on the mechanical properties of ASTM type I specimens manufactured via stereolithography. *Rapid Prototyp J* 2012; 18(5): 374-388.
25. Imetrum. Video gauge™ - how it works, <https://www.imetrum.com/video-gauge/how-it-works/> (2012, accessed 18 June 2019)
26. Dong G, Tang Y, Zhao YF. A survey of modeling of lattice structures fabricated by additive manufacturing. *J Mech Des* 2017; 139(10): 100906.
27. Ravari MRK, Kadkhodaei M, Badrossamay M, et al.

Numerical investigation on mechanical properties of cellular lattice structures fabricated by fused deposition modeling. *Int J Mech Sci* 2014; 88: 154-161.

28. Campoli G, Borleffs MS, Yavari SA, et al. Mechanical properties of open-cell metallic biomaterials manufactured using additive manufacturing. *Mater Des* 2013; 49: 957-965.

29. Labeas GN, Sunaric MM. Investigation on the static response and failure process of metallic open lattice cellular structures. *Strain* 2010; 46(2): 195-204.

30. Luxner MH, Stampfl J, Pettermann HE. Finite element modeling concepts and linear analyses of 3D regular open cell structures. *J Mater Sci* 2005; 40(22): 5859-5866.

31. ABAQUS C. Analysis user's manual, 2017.

32. Simulia user assistance. Abaqus-Choosing a beam element,

https://help.3ds.com/2017/english/dssimulia_established/simacaeelmrefmap/simaelm-c-beamelem.htm?contextscope=all (2017, accessed 20 June 2019)

33. Ahmadi SM, Campoli G, Yavari SA, et al. Mechanical behavior of regular open-cell porous biomaterials made of diamond lattice unit cells. *J Mech Behav Biomed. Mater* 2014; 34: 106-115.